remote sensing

MDPI

Article

Velocity Dealiasing for 94 GHz Vertically Pointing MMCR with Dual-PRF Technique

Hai Lin [1], Jie Wang [1] and Junxiang Ge [1,2,3,*]

[1] School of Electronic and Information Engineering, Nanjing University of Information Science & Technology, Nanjing 210044, China; eleclin@nuist.edu.cn (H.L.); wangjie@nuist.edu.cn (J.W.)
[2] Institute of Electronics Information Technology and System, Nanjing University of Information Science & Technology, Nanjing 210044, China
[3] Jiangsu Key Laboratory of Meteorological Observation and Information Processing, Nanjing University of Information Science & Technology, Nanjing 210044, China
* Correspondence: jxge@nuist.edu.cn

Abstract: Velocity aliasing is unavoidable for millimeter-wave cloud radar (MMCR) due to its short wavelength. In the vertically pointing MMCR, a special aliasing state called half-folding will cause the traditional postprocessing dealiasing methods used for weather radar, including the dual-PRF method, to fail. In this paper, we propose a method that applies the dual-PRF technique to spectral dealiasing. By utilizing the property that the true velocity difference between peaks should be the same in both PRFs, our method is able to solve a special case of half-folding caused by multiple peaks, which is ignored by other spectral dealiasing methods. The special case, which we call implicit half-folding, occurs in the presence of multiple peaks in a Doppler power spectrum, where none of the peaks are folded, and they appear to be in the same Nyquist interval, whereas the peaks are actually not in the same Nyquist interval. Observations from a 94 GHz vertically pointing MMCR called TJ-II were used to demonstrate various aliasing cases, including the implicit half-folding case. As a result, our method successfully solved all aliasing cases while the other method failed when the implicit half-folding case occurred.

Keywords: velocity aliasing; MMCR; dual PRFs; spectral dealiasing; half-folding

check for updates

Citation: Lin, H.; Wang, J.; Ge, J. Velocity Dealiasing for 94 GHz Vertically Pointing MMCR with Dual-PRF Technique. *Remote Sens.* **2023**, *15*, 5234. https://doi.org/10.3390/rs15215234

Academic Editors: Jing Li, Yannian Zhu, Zeen Zhu and Jinming Ge

Received: 28 September 2023
Revised: 31 October 2023
Accepted: 2 November 2023
Published: 3 November 2023

Copyright: © 2023 by the authors. Licensee MDPI, Basel, Switzerland. This article is an open access article distributed under the terms and conditions of the Creative Commons Attribution (CC BY) license (https://creativecommons.org/licenses/by/4.0/).

1. Introduction

Clouds cover approximately two-thirds of the Earth's surface and play a significant role in both the global hydrological cycle and the climate through Earth's radiated energy budget [1,2]. Clouds constitute the largest single source of uncertainty in climate prediction [3]. Therefore, the study of clouds is integral to meteorological and climate research. Cloud research encompasses a vast and intricate domain, spanning from macroscopic, such as cloud amount, cloud shape, cloud height, and cloud velocity detection, to microscopic cloud particle physics, chemistry, optics, radiation characteristics, etc. Cloud sensing is the foundation of cloud research, and remote sensing emerges as the primary methodology for cloud observation due to the difficulty of physically reaching the clouds.

Among the instruments of remote sensing, the millimeter-wave cloud radar (MMCR) is a unique tool for investigating cloud systems. MMCRs offer a higher sensitivity than lower-frequency radars and a better cloud penetration than Lidar [4]. MMCRs primarily operate within the Ka-band (35 GHz, with a wavelength of 8 mm) and W-band (94 GHz, with a wavelength of 3 mm), and their excellent performance in cloud detection has been demonstrated by many studies [5–9]. The superior performance of MMCRs can be largely attributed to their shorter wavelength. Cloud particle sizes are typically small, and Rayleigh scattering is valid, that is, the amount of scattering is inversely proportional to the fourth power of the wavelength. Therefore, the 94 GHz MMCR has a higher sensitivity than the 35 GHz one.

A vertically pointing radar is the base form of MMCR because of the simple mechanical setup. This radar is suitable for long-term monitoring of clouds. The Doppler velocity observed by vertically pointing radars includes great information on the terminal fall velocity of the cloud particles [10]. In terms of velocity detection, however, the shorter wavelength of the MMCR becomes a limitation where the max unambiguous velocity (also called the Nyquist velocity) of the Doppler radar follows Equation (1).

$$V_{max} = \frac{\lambda \cdot PRF}{4} \tag{1}$$

The Nyquist velocity is determined by the wavelength λ and the pulse repetition frequency (PRF). For a specific MMCR, the wavelength is fixed, and the PRF becomes the sole adjustable parameter. However, the PRF is also associated with the detection range. In the trade-off between range and velocity ($R_{max}V_{max} = c\lambda/8$), most tend to favor range, as range aliasing is more challenging to mitigate with a body target like a cloud. Given this consideration, the PRF cannot exceed 10 kHz, corresponding to a PRT (pulse repetition time) of no less than 100 µs, for a vertically pointing MMCR with a conventional detection range of 15 km. The corresponding Nyquist velocity for a 94 GHz MMCR is about 8 m· s^{-1}. Even though the vertical velocity of the cloud is much smaller than its horizontal velocity, 8 m· s^{-1} is not enough to cover all the scenarios, such as a strong convection and turbulence, and then velocity aliasing occurs.

Velocity aliasing, also known as velocity folding, is a fundamental sampling issue arising when the Nyquist velocity sampling interval ($\pm V_{max}$) is less than the full range of naturally occurring velocities, causing the erroneous appearance of higher velocities within the sampling interval. Any true velocity, V_t, appears within the interval from $-V_{max}$ to $+V_{max}$, with the value V_i, which is related to the true velocity by Equation (2), where n is an integer. Therefore, a given measured velocity v_i may be caused by many values of the true velocity V_t. The process of finding the correct n is called velocity dealiasing.

$$V_t = V_i \pm 2nV_{max} \tag{2}$$

Velocity dealiasing has historically been the focus of numerous postprocessing algorithms [11–17]. These algorithms work on the principle of maintaining the continuity of cloud velocity between neighboring range gates or time bins. The differences between these postprocessing methods mainly lie in the choice of thresholds, neighboring bins, and reference velocities.

An alternative to the postprocessing is to extend the Nyquist velocity. According to Equation (1), the Nyquist velocity is determined by the wavelength and PRF, where the wavelength is fixed for a specific radar, while the PRF is also limited by the detection range. To overcome the limitation of the PRF, multiple PRFs, usually two PRFs, are used, which is a common method in military radar [18]. There are two common methods, the staggered-PRF (PRT) method [19,20] and the dual-PRF method [21]. The staggered-PRF method changes the PRF between pulses to create a nonuniform time series, while the dual-PRF method collects two uniform time series sequentially at different PRFs. The dual-PRF method needs an inherent requirement of spatial continuity over the combined interval so that the continuity deteriorates in high-shear regions of scanning radar. Therefore, the staggered-PRF method is more suitable for scanning radars while the dual-PRF method is suitable for vertically pointing radars. Compared to conventional postprocessing methods, dual-PRF or staggered-PRF methods are more reliable because they do not rely on the continuity of cloud velocities; instead, they place demands on the radar's operational or hardware aspects. Most of these velocity dealiasing methods mentioned above, including the dual-PRF method, were primarily developed for conventional weather radars. These methods rely on the measured Doppler mean velocity V_i and the basic principle given by Equation (2). However, when dealing with a vertically pointing MMCR, a major issue arises where the measured Doppler mean velocity V_i may break the basic principle. There is a substantial

difference between the velocities observed by a weather radar and a vertically pointing MMCR. Velocity in a weather radar is caused by the ambient wind field, mainly horizontal winds. The velocity of the particle swarm can be regarded as a target object, while the velocity in a vertically pointing MMCR is caused by the falling of different particles and updraft (or downdraft). The Doppler velocity's spectral width in a vertically pointing MMCR is wider and cannot be considered a target object, leading to a phenomenon called half-folding in specific cases.

Half-folding occurs when the full range of true velocity lies in both adjacent Nyquist intervals. Half-folding will result in an incorrect V_i, breaking Equation (2). Consequently, any velocity dealiasing methods based on the erroneous V_i will surely lead to inaccurate results. To obtain the correct dealiased velocity, half-folding must be addressed at the Doppler power spectrum stage before calculating V_i.

Several spectral dealiasing methods have been proposed to deal with half-folding [22–24]. The one closer to the reference velocity of the previous range gate was selected as the dealiased velocity. Maahn [22] performed a periodic expansion of the original Doppler spectrum ($-V_{max}$, V_{max}) to the new one ($-3V_{max}$, $3V_{max}$). As a result, the new spectrum could contain up to three peaks with different Doppler velocities. To find the correct peak, the initial reference velocity was derived by an empirical formula between Z_e (calculated by the original spectrum) and V_t. The peak closest to the reference velocity was considered the most likely one. Then, Maahn chose some of the most likely peaks with the smallest differences as the trusted peaks. Then, the iteration started by using the trusted peaks at the new reference of their neighboring range gates. Both these methods, similar to postprocessing techniques used in weather radar, are based on the cloud velocity continuity between neighboring range gates. Therefore, they have the same drawbacks as those techniques, particularly in strong convective conditions where the true velocity of neighboring range gates may exceed the continuity threshold, leading to a misjudgment of the Nyquist interval (related to the value n). Additionally, an outlier result of a bin can affect all the following bins due to the gate-by-gate iterative algorithm. For the dual-PRF technique, there are limited studies on the use of the dual-PRF technique in spectral dealiasing.

In this paper, we propose a highly reliable velocity dealiasing method using the dual-PRF technique. The method involves two stages: the preprocessing stage, which is spectral dealiasing using the Doppler power spectrum data, and the postprocessing stage, which employs dual-PRF processing with base data (time-height data). The properties brought by the dual PRFs are applied to both stages. In the preprocessing stage, spectral dealiasing addresses the half-holding and fixes the V_i calculated by the Doppler spectral moment to meet the basic principle in Equation (2). In the postprocessing stage, the dual-PRF processing, similar to that used in weather radar, is meant to derive the final true velocity. Therefore, in this paper, the spectral dealiasing that introduced the property of consistency of the velocity difference between PRFs, brought by the dual PRFs, is detailed. The dual-PRF technique is briefly described in Section 2. The half-folding is described in Section 3. Our method is detailed in Section 4. Several half-folding cases observed by the TJ-II cloud radar [25] are used to demonstrate the adaptability of our dealiasing method in Section 5. In Section 6, we compare our method with others in terms of overall results and statistical data.

2. Dual PRF

In this section, the concept of dual-PRF processing is briefly described. V^h_{max} and V^l_{max} are the Nyquist velocities associated with the high and low PRFs, respectively. The same true velocity V_t will appear as different velocities V^h and V^l when folded back to the high and low Nyquist velocity intervals, respectively. By combining the two velocity measurements, the equivalent Nyquist velocity interval can be extended. The new extended Nyquist velocity V^e_{max} can be represented by [26]

$$V^e_{max} = \frac{V^h_{max} V^l_{max}}{V^h_{max} - V^l_{max}} \tag{3}$$

For convenience, the ratio of the two PRFs is chosen as a function of an integer factor N in the form

$$\frac{PRF_h}{PRF_l} = \frac{V_{max}^h}{V_{max}^l} = \frac{N+1}{N} \tag{4}$$

Then, the extended Nyquist velocity can be represented by

$$V_{max}^e = NV_{max}^h = (N+1)V_{max}^l \tag{5}$$

The velocity estimate $\overline{V}_f$ follows the principle of Equation (2) and can be simply derived from the two measured velocities $\overline{V}^h$ and $\overline{V}^l$ of the high and low PRFs, respectively, which can be expressed by [27]

$$\overline{V}_f = (N+1)\overline{V}^l - N\overline{V}^h \tag{6}$$

It is hard to apply the dual-PRF processing directly into the Doppler power spectrum as spectral dealiasing. This is because, in the base data, the velocities have already been integrated into a single value (Doppler mean velocity), and only one-to-one correspondences need to be handled. However, in the Doppler power spectrum, there are multiple velocity spectral line values, where the many-to-many correspondences are hard to handle.

3. Half-Folding

Different from the point target radar, the subject of cloud radar, the cloud, is a body target composed of multiple particles. The motion of these particles within the cloud is nonuniform, particularly in a vertically pointing cloud radar. The velocity of the cloud in a vertically pointing cloud radar consists of the falling velocity of different particles and the updraft (or downdraft), leading to a broadening in the velocity spectral width. When part of the cloud velocity goes beyond the Nyquist interval, half-folding occurs. The higher-velocity part goes beyond the current Nyquist interval and then is folded back into the negative interval, while the lower part remains in the positive interval, as shown in Figure 1c. The red dashed lines indicate the Nyquist interval. With a further increase in velocity (equivalent to a decrease in V_{max}), it goes to a full folding, as shown in Figure 1d.

When half-folding occurs, the Doppler mean velocity V_i calculated by the Doppler spectral first moment is biased and breaks Equation (2). For example, if the true Doppler mean velocity is precisely equal to the Nyquist velocity V_max and the spectrum is equally divided between the left and right sides, as shown in Figure 1c, the directly calculated Doppler mean velocity is zero and there is no integer n that satisfies Equation (2). For full-folding cases, the directly calculated Doppler mean velocity satisfies Equation (2) and can be used to derive the true velocity by postprocessing. Therefore, spectral dealiasing is mainly used to solve the half-folding case in our method.

In fact, there are significantly more half-folding cases than full-folding cases in the 94 GHz vertically pointing MMCR observations. Therefore, for high-velocity scenes, such as those with precipitation or strong convection, the presence or absence of spectral dealiasing has a significant impact on the data quality of MMCR. Several spectral dealiasing methods have been proposed [22–24]. As noted in Section 1, both Zheng and Maahn's iterative methods have the drawback of error conduction. Additionally, they only consider cases with a single peak, which is not always the case in real observations. It is not rare to have two peaks in a single Doppler power spectrum [28–31]. These methods may fail in such cases. For example, depending on the different Nyquist velocities and the velocity difference between the peaks, the Doppler power spectrum may exhibit one of three cases. One is that both peaks are in the same Nyquist interval and neither is folded, two is that one of the peaks is folded, and three is that the two peaks are in different Nyquist intervals and neither is folded. We call case two explicit half-folding and case three implicit folding. Case three looks the same as case one, which will be ignored by Zheng's method. Therefore,

distinguishing between case three and case one is critical for spectral dealiasing in cases with two peaks.

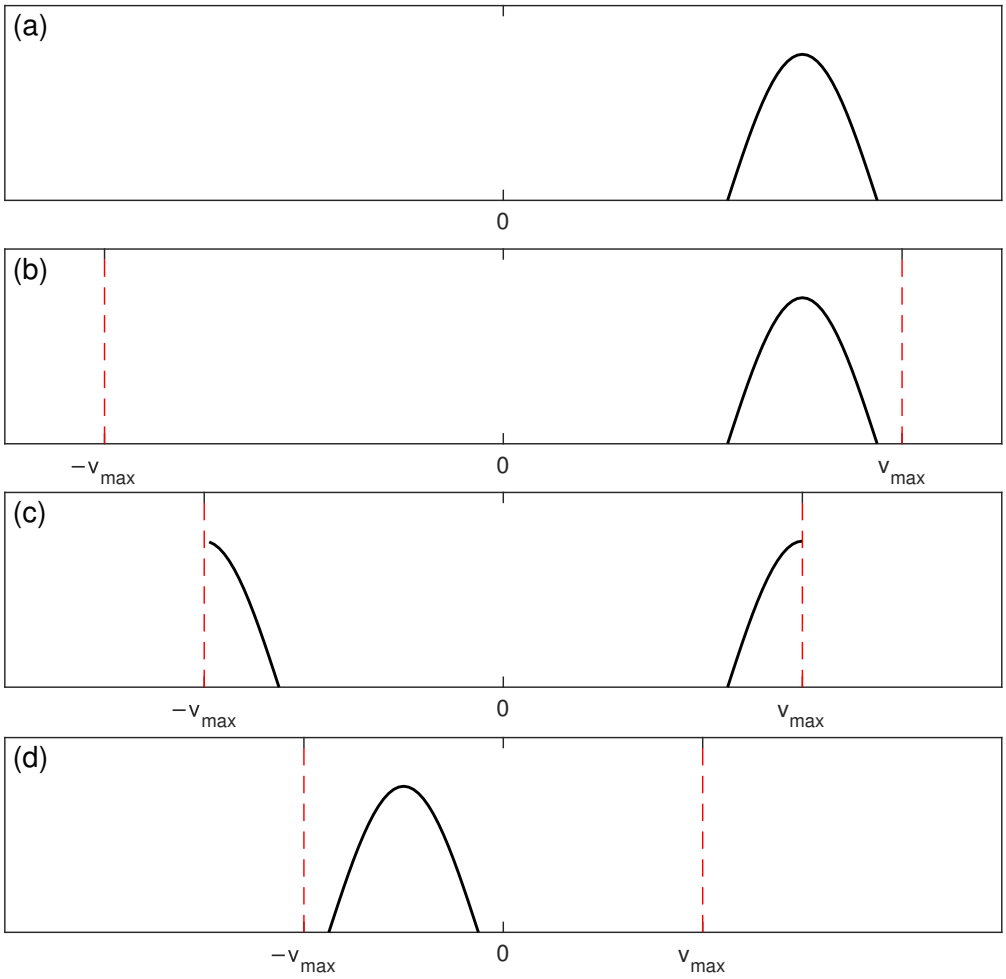


Figure 1. Example of folding cases with a single peak with different V_{max}'s. (**a**) Original Doppler spectrum. (**b**) Nonfolding case, (**c**) half-folding case, and (**d**) full-folding case.

4. Methodology

The proposed method consists of two stages. In the spectral dealiasing stage, we use the physical property that comes with the dual PRFs to solve the half-folding. Our spectral dealiasing method can detect and resolve all types of half-folding cases, including the implicit half-folding. In the postprocessing stage, we use the conventional dual-PRF processing method.

4.1. Spectral Dealiasing

Unlike other spectral dealiasing methods under a single PRF, which restores the final mean velocity V_t directly, our spectral dealiasing process aims to eliminate the effect of the half-folding and restore a Doppler mean velocity V_i that meets the principle of Equation (2). Therefore, the key to our spectral dealiasing lies in the detection of the half-folding and its dealiasing. First, we need to determine the number of separated peaks in the Doppler power spectrum. The schematic diagram is shown in Figure 2.

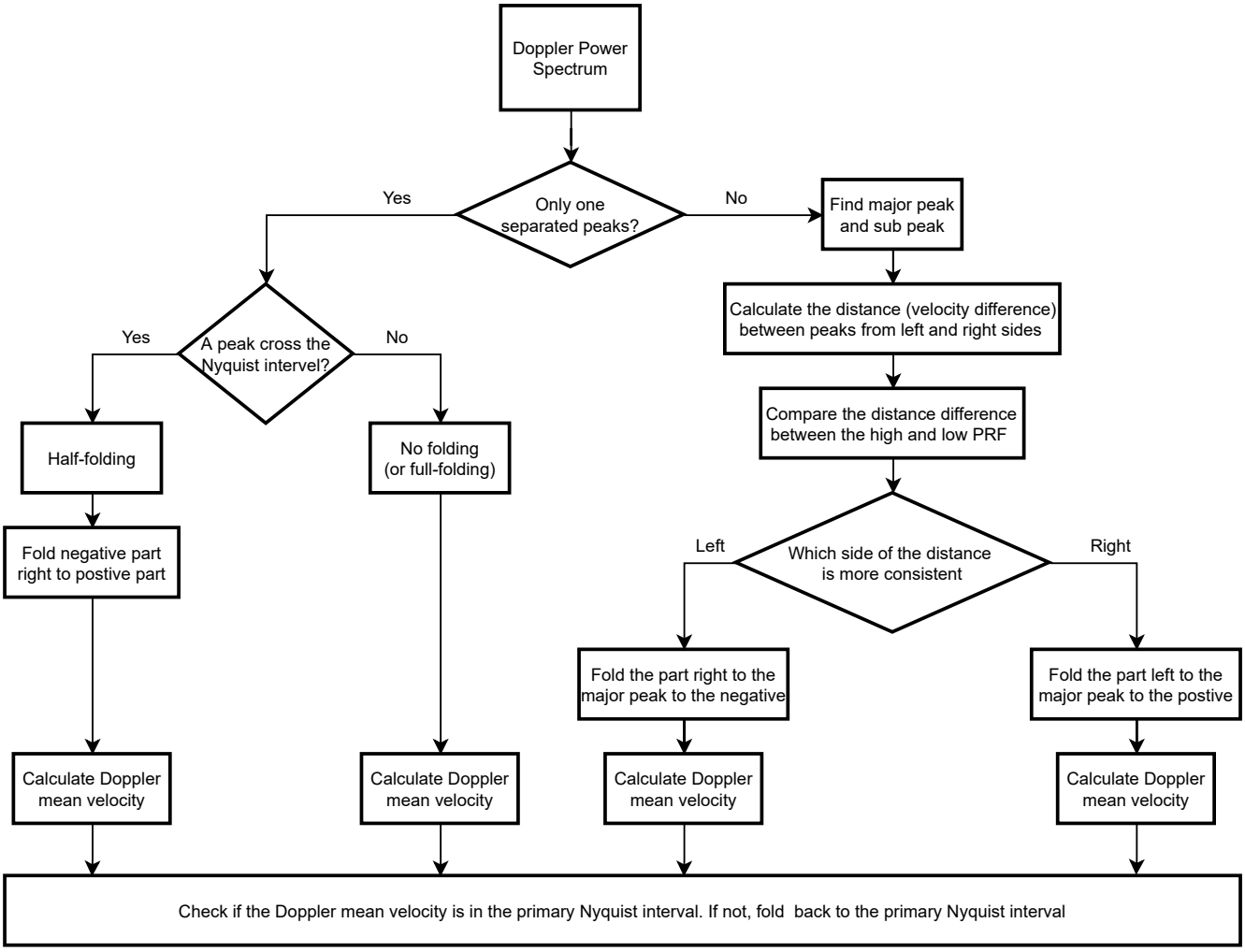


Figure 2. Schematic diagram of spectral dealiasing.

When dealing with single-peak cases, the process is relatively straightforward. Only one type of half-folding occurs, wherein the cloud signal crosses the Nyquist interval. The property of the dual PRFs is not used. The process is similar to Zheng's [23] one. Half-folding is detected when the right endpoint of the cloud signal reaches $+V_{max}$ and the left endpoint reaches $-V_{max}$. For convenience, we move the left part to the right side of the right part. Then, we calculate the dealiased Doppler mean velocity according to the dealiased spectrum. If the dealiased Doppler mean velocity is over the positive Nyquist velocity V_{max}, we fold it back to the primary Nyquist interval by subtracting $2V_{max}$. Again, this is for the convenience of dual-PRF processing at the base data stage.

For cases with multiple peaks, which are almost always two peaks, the process is more complicated. There are multiple half-folding cases. Figure 3 shows an example of the same original velocity that produces different half-folding cases depending on the different Nyquist velocities.

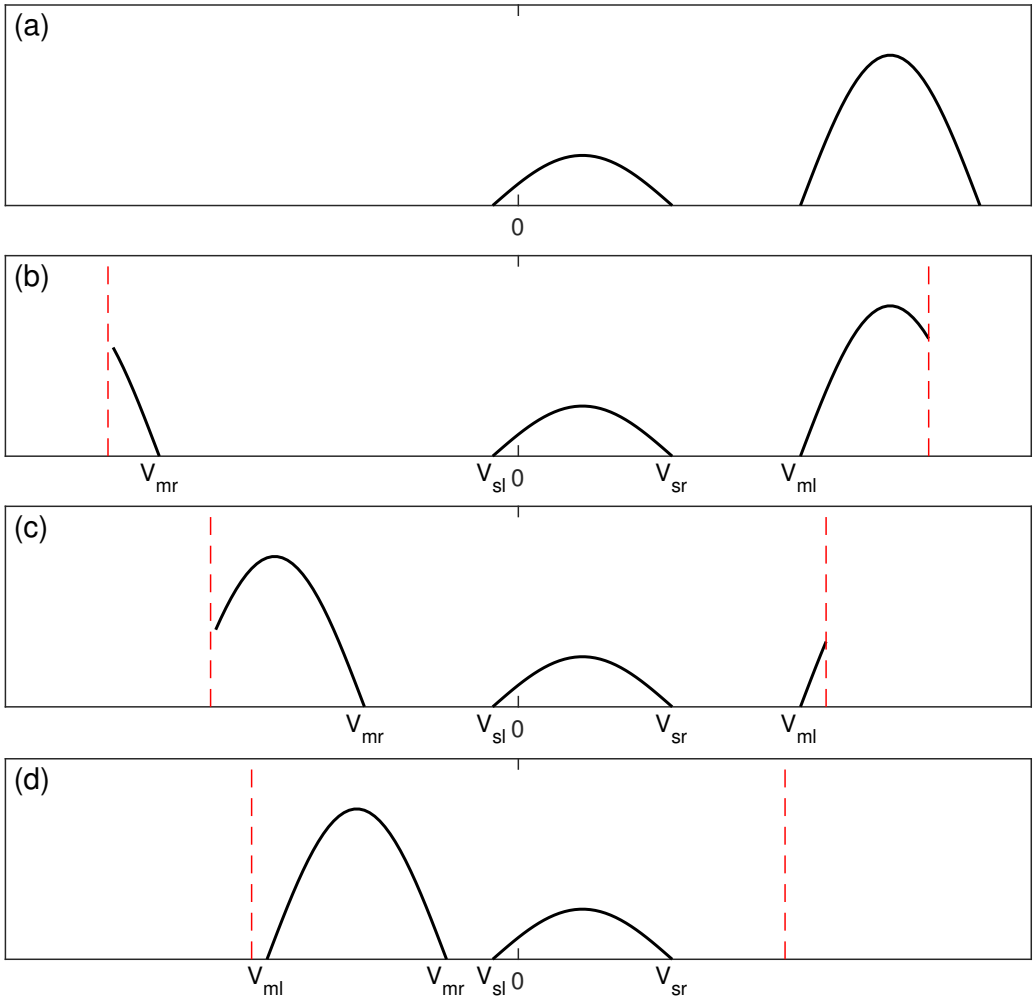


Figure 3. Example of half-folding cases with two separated peaks. (**a**) Original Doppler spectrum. (**b**–**d**) folding cases with different V_{max}.

Figure 3a denotes an original Doppler power spectrum. Figure 3b–d show various half-folding cases with different Nyquist velocities where the red dashed line indicates the Nyquist interval. When half-folding occurs, should we move the left part of the folded peak to the right of the right part or vice versa? That is to say, how do we determine the positional relationship between the two peaks after dealiasing? In the case of Figure 3b, it is natural to assume that the unfolded peak should lie to the left of the folded peak after dealiasing because it is closer to the right part of the folded peak. When it comes to Figure 3c, the unfolded peak is equidistant from both sides, making it difficult to determine whether the unfolded peak should be to the left or right of the folded peak after dealiasing. As the Nyquist velocity decreases further, the unfolded peak will be closer to the left side, leading to a misjudgment. What is more, when the Nyquist velocity decreases to the point where the case in Figure 3d occurs, it seems that no half-folding occurs. This is the most misleading case of implicit half-folding we mentioned above.

Therefore, the presence of a visible folded peak is no longer the most important. The key lies in the positional relationship between the two peaks, that is, whether the two peaks are in the same Nyquist interval, which is difficult to determine from a single-PRF result, especially for the case in Figure 3d. In Lin's method [25], the idea is to compare the distance (velocity difference) between the two peaks and identify the smaller distance as the correct one, while the larger distance is a result of Nyquist folding. It is usually effective in most cases but fails in the rare case where the true distance is equal to or greater than the folding distance, as seen in Figure 3c,d. It is not a reliable method. The probability

of failure increases with a lower PRF because the folding distance V_{dN} is related to the Nyquist velocity. This method limits the PRF choice to some extent.

Our improved method still solves the aliasing problem by finding out the true distance. The improvement is that instead of relying on empirical relationships, we rely on the physical property of dual PRFs, i.e., the true distances remain consistent, while the folding distances vary under different PRFs due to Nyquist folding. The following are the specific steps.

The first is to resolve the explicit half-folding when there is a folded peak, the same as what is done in the single-peak case. Then, we find the major (or strongest) peak as the reference. We calculate the distance (velocity difference) from the subpeak (second strongest) to the left and right of the major peak, V_{dl} and V_{dr}, respectively. One should be the true distance V_{dt} and the other is the folding distance V_{dN} caused by the Nyquist folding, which varies with the Nyquist velocity (PRF). It can be expressed by Equation (7) or Equation (8). $\overline{V}_m$ and $\overline{V}_s$ denote the Doppler mean velocity of the major peak and subpeak, respectively.

$$\begin{aligned} V_{dl} &= \overline{V}_m - \overline{V}_s \\ V_{dr} &= \overline{V}_s - \overline{V}_m + 2V_{max} \end{aligned} \tag{7}$$

$$\begin{aligned} V_{dl} &= \overline{V}_m - \overline{V}_s + 2V_{max} \\ V_{dr} &= \overline{V}_s - \overline{V}_m \end{aligned} \tag{8}$$

Equation (7) is used for $\overline{V}_m > \overline{V}_s$ while Equation (8) is used for $\overline{V}_m < \overline{V}_s$. This is to make both distances positive, and it also brings in the property that $V_{dl} + V_{dr} = 2V_{max}$.

By comparing the consistency of distances under the two PRFs, $V^h_{dr} - V^l_{dr}$ and $V^h_{dl} - V^l_{dl}$, we can determine whether the subpeak should be placed to the left or right side of the major peak. The superscripts h and l denote the results for high and low PRFs, respectively. One difference should be close to 0 and be determined as the true distance. The other should be $2(V^h_{max} - V^l_{max})$ and be determined as the folding distance. Then, the split point can be any point in the interval associated with the folding distance. Here, we use the median. The interval for the left distance is (V_{sr}, V_{ml}) if $V_{ml} > V_{sr}$, or (V_{sr}, V_{max}) and $[-V_{max}, V_{ml})$ if $V_{ml} < V_{sr}$. The interval for the right distance is (V_{mr}, V_{sl}) if $V_{mr} < V_{sl}$, or (V_{mr}, V_{max}) and $[-V_{max}, V_{sl})$ if $V_{mr} < V_{sl}$. V_{ml} and V_{mr} are the left and right endpoints of the major peak, respectively. V_{sl} and V_{sr} are the same for the subpeak. Then, we divide the original Doppler power spectrum into two segments by split point and shift the left segment to the right of (V_{max}). Finally, we calculate the final dealiased Doppler mean velocity. Alternatively, we can shift the right segment to the left of $-V_{max}$. The difference between the Doppler mean values calculated by these two shifting methods is $2V_{max}$ and therefore will not affect the final value which is in the primary Nyquist interval $(-V_{max}, V_{max}]$. For convenience, we shift the left segment.

Our spectral dealiasing fixes the failure of the basic dealiasing principle of Equation (2) due to the half-folding and obtains the $\overline{V}^h$ and $\overline{V}^l$ that meet the Equation (2). However, these results do not represent the final output because the spectral dealiasing process does not identify the correct Nyquist interval (the value of n) where the true velocity is located. It is the work of the conventional dual-PRF processing at the base data stage.

4.2. Postprocessing

The dual-PRF processing at the base data stage would be no different from the ones in weather radar. Here is a brief description. First, based on the spectral dealiased Doppler mean velocity, $\overline{V}^h$ and $\overline{V}^l$, Equation (4) is used to calculate the primary velocity estimate. If a velocity estimate falls outside of the new equivalent Nyquist interval $\pm V^e_{max}$, it should be folded back into the primary Nyquist interval by addition or subtraction of $2V^e_{max}$. However, the primary velocity estimate is obtained by the differencing of two Doppler mean velocities and its standard deviation will be amplified [27]. Thus, it is not a suitable

velocity estimator [26]. The primary velocity estimate is merely used to indicate the Nyquist interval (n) that the original Doppler mean velocity belongs to. The dealiased velocity is then obtained with the standard deviation of the original Doppler mean velocity by Equation (2).

5. Materials

5.1. TJ-II Cloud Radar

TJ-II is a vertically pointing MMCR developed by the Nanjing University of Information Science & Technology (NUIST). It is a pulse Doppler radar working at 94 GHz. TJ-II features a 6 W solid-state power amplifier (SSPA) and employs a single antenna. This design enhances its compactness, making it suitable for ground-based observations as well as mobile applications, such as emergency monitoring of extreme weather events.

In routine observations, TJ-II uses only the single-PRF mode to maximize the integration time (more accumulation times) to improve the cloud detection sensitivity. For precipitation or some extreme weather, however, the vertical velocity of clouds increases, resulting in velocity aliasing in observations. To improve the velocity measurement capability, TJ-II uses the dual-PRF technique, which has the disadvantage of reducing the detection sensitivity (a reduction in integration time). However, in such scenarios, the cloud echoes are typically stronger, and the detection sensitivity is not a primary concern. The two PRFs used in TJ-II are 8.333 kHz and 6.667 kHz, corresponding to PRTs of 120 µs and 150 µs, respectively. The ratio is 5:4. The corresponding Nyquist velocities are approximately 6.65 m s^{-1} and 5.32 m s^{-1} for V^h_{max} and V^l_{max}, respectively. The equivalent Nyquist velocity V^e_{max} is 26.60 m s^{-1}.

5.2. Analysis of Observation Data

The observations were conducted on 15 July 2023, from 13:00 to 14:00 UTC+8 at NUIST, Nanjing, China. The weather condition was a short period of precipitation. The unprocessed Doppler mean velocities are shown in Figure 4. There are a large number of corresponding regions with significant velocity differences (color differences) between the two PRFs' results, which indicates the presence of velocity aliasing. There are also significant half-folding cases and different cases.

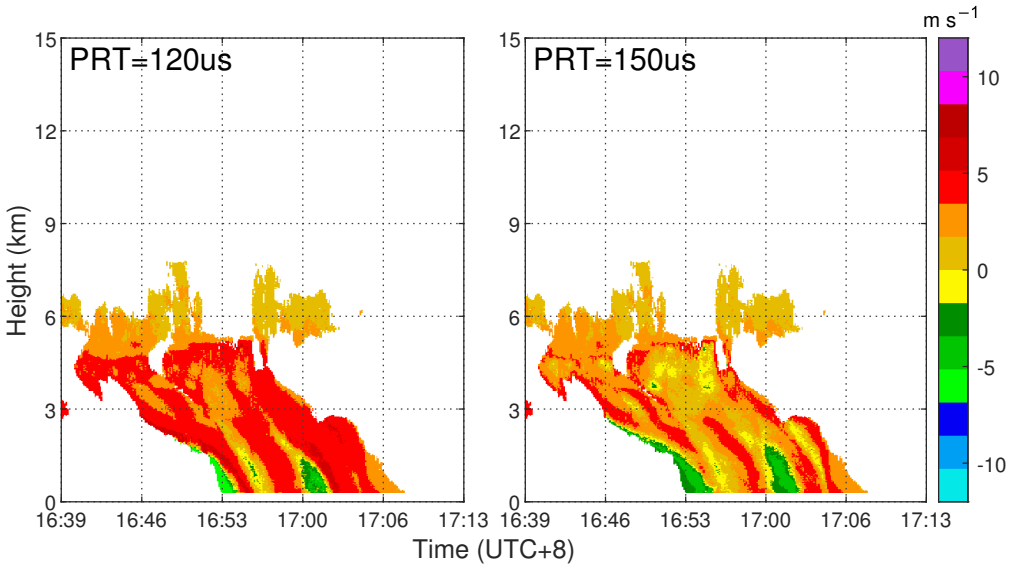


Figure 4. The original Doppler mean velocity measurement by TJ-II.

5.3. Case A

For example, a frame of velocity profile around 16:51 is shown in Figure 5a.

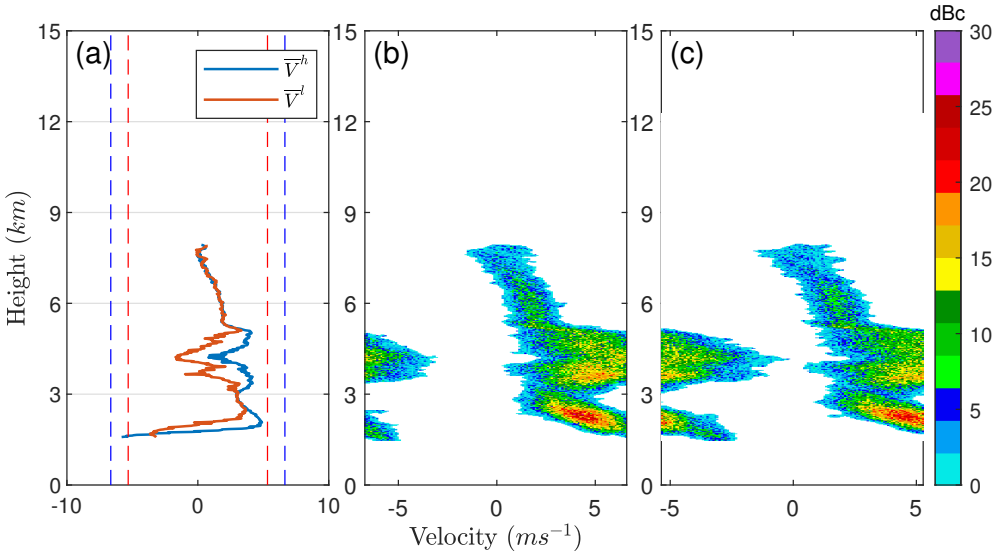


Figure 5. A frame from the TJ-II observation with dual PRFs. (**a**) Unprocessed Doppler mean velocity profile. (**b**) The corresponding Doppler power spectrum of the high PRF and (**c**) the corresponding Doppler power spectrum of the low PRF.

The blue line denotes the velocity profile for the high PRF, and the blue dash line indicates its corresponding Nyquist interval, while the red ones are for the low PRF. It is evident that the velocity aliasing commenced at about 5.15 km for the low PRF. $\overline{V}^l$ started to decrease while $\overline{V}^h$ still increased, and the aliasing type was a half-folding type. $\overline{V}^l$, which should have transitioned directly from positive to negative, just started to decrease. Another distinctive feature about the half-folding is that neither $\overline{V}^h$ nor $\overline{V}^l$ reached their Nyquist velocity V^h_{max} and V^l_{max}, respectively.

Figure 5b,c show the corresponding Doppler power spectrum of the profile for the high and low PRFs, respectively. The half-folding can be visualized. For the low PRF, the half-folding started at about 5.15 km and transformed into a nonfolding at about 3 km, then another half-folding started at 2.6 km and transformed into a full folding at 1.7 km. For the high PRF, the half-folding started at about 5.05 km and transformed into a nonfolding at about 3.4 km, then another half-folding started at 2.5 km and transformed into a full folding at 1.6 km. When both spectrums of high and low PRFs were nonfolding, their profiles matched well, such as the section above 5.15 km and between 3 km and 2.5 km. In other cases, they were mismatched. In the segment from 4 km to 3.6 km, the Doppler power spectrum of the low PRF was half in the positive and half in the negative region, which is manifested in the velocity profile by its variation around 0 m s^{-1}. The conventional postprocessing dealiasing method, based on the single PRF, is incapable of detecting the aliasing because the velocity difference of neighboring range gates is lower than the threshold to detect an aliasing. A common threshold of the velocity difference used to detect the aliasing is one times the Nyquist velocity [14], while in this profile, the maximum velocity difference for the low PRF was only 0.22 of its Nyquist velocity. As mentioned above, the half-folding broke Equation (2) and the conventional dual-PRF processing based on it only yielded incorrect results, as shown in Figure 6c.

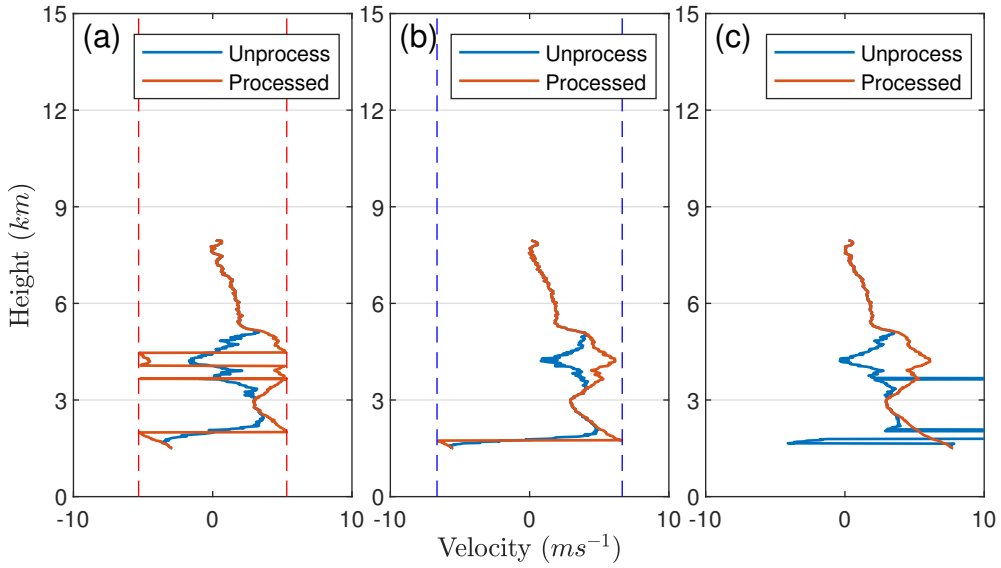


Figure 6. Comparison between the results of dual-PRF processing with and without half-folding preprocessing. (**a**) The Doppler mean velocities with and without half-folding preprocessing for the low PRF (**b**), the same as (**a**) for the high PRF. (**c**) The final dealiasing results of dual-PRF processing with and without half-folding preprocessing.

In Figure 6a,b, we can see the changes in Doppler mean velocity of the high and low PRFs after our spectral dealiasing, respectively. The dashed lines indicate their corresponding Nyquist intervals. The dealiased Doppler mean velocity can now touch the Nyquist velocity. A comparison of the dual-PRF dealiasing processing with and without the half-folding dealiasing (spectral dealiasing) is shown in Figure 6c. The results of the dual-PRF processing without spectral dealiasing show significant errors in the segment where the half-folding occurs. Only the results of three segments, above 5.15 km, from 3 to 2.6 km, and below 1.6 km, are correct. The states of the first two segments in both PRFs are both nonfolding, while the last one is full folding. Whenever half-folding occurs in any one of the Doppler power spectrums, the result of the dual-PRF processing produces a large deviation. The results of the dual-PRF processing with our spectral dealiasing appear more reasonable and align with human judgment.

5.4. Case B

In case A, we showed the impact of half-folding on the Doppler mean velocity and the final dealiasing results. Case B shows a case with two peaks in one range gate, as shown in Figure 7.

There are two parts of cloud signals in this frame. There was no aliasing in the upper cloud, therefore the unprocessed Doppler mean velocities of high and low PRFs were in good agreement. The lower layer, on the other hand, extended into the radar's blind spot, with the solid red signal at the bottom indicating the presence of precipitation. Naturally, the velocity aliasing occurred and contained a variety of half-folding cases. The half-folding started from 3.4 km for the low PRF and 2.9 km for the high PRF. At first, the half-folding was a simple single-peak case and as the precipitation signal appeared, it turned into a two-peak case. As the cloud signal disappeared, the Doppler spectrum suddenly turned back to a single-peak case without aliasing. With the precipitation velocity increasing, half-folding with a single-peak case appeared again. Figure 8 shows the spectral dealiasing results using our method and Zheng's method. Figure 9 shows the dealiased Doppler power spectrum using our method and Zheng's method. To better show the difference between Zheng's method and ours, we have not folded back the velocities beyond the primary Nyquist interval in Figure 8a (the mutation lines would interfere with the observation).

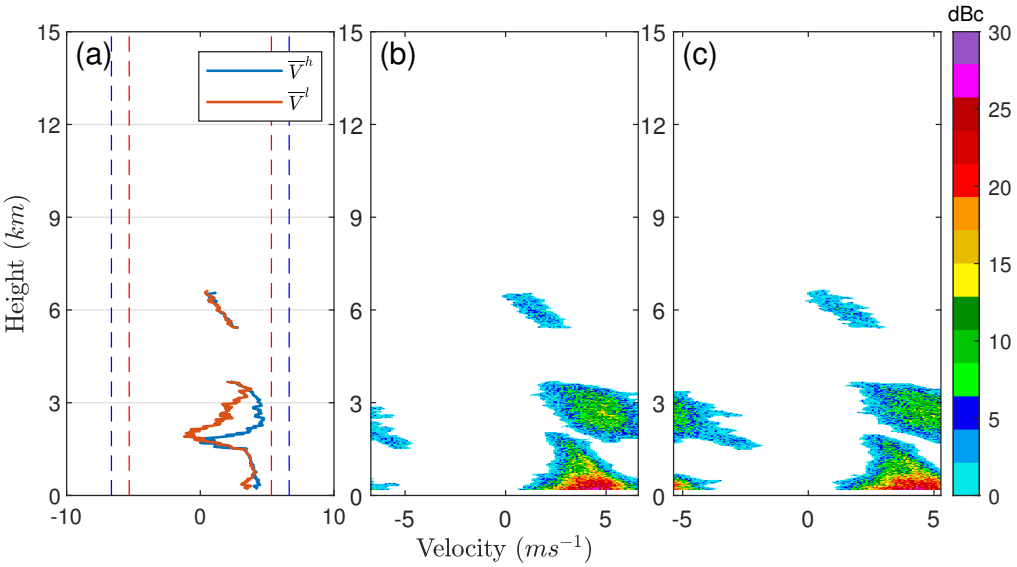


Figure 7. Another slice from the TJ-II observation with dual PRFs. (**a**–**c**) are the same as in Figure 5.

Our method and Zheng's method performed similarly for the single-peak case. Both Zheng's and our method could resolve the two-peak case with one of the peaks crossing the Nyquist interval. However, when the folded peak turned unfolded with the increase in velocity, Zheng's method thought there was no half-folding and directly calculated the Doppler mean velocity, such as the red rectangle area in Figure 9(a2,b2).

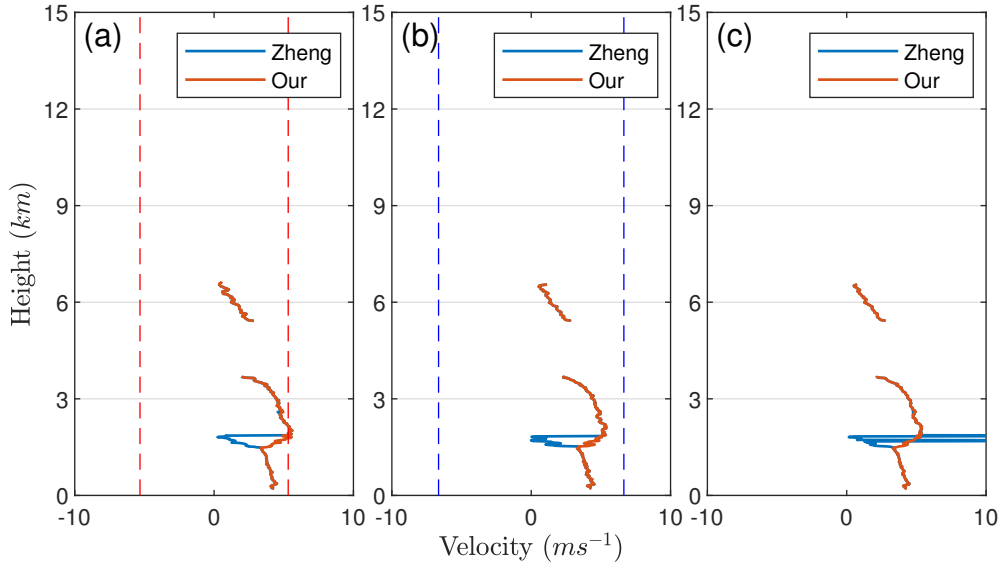


Figure 8. Comparison between the results of dual-PRF processing by our method and Zheng's. (**a**) Spectral dealiased Doppler mean velocities for the low PRF. (**b**) Spectral dealiased Doppler mean velocities for the high PRF. (**c**) The final dealiasing results of the dual-PRF processing result.

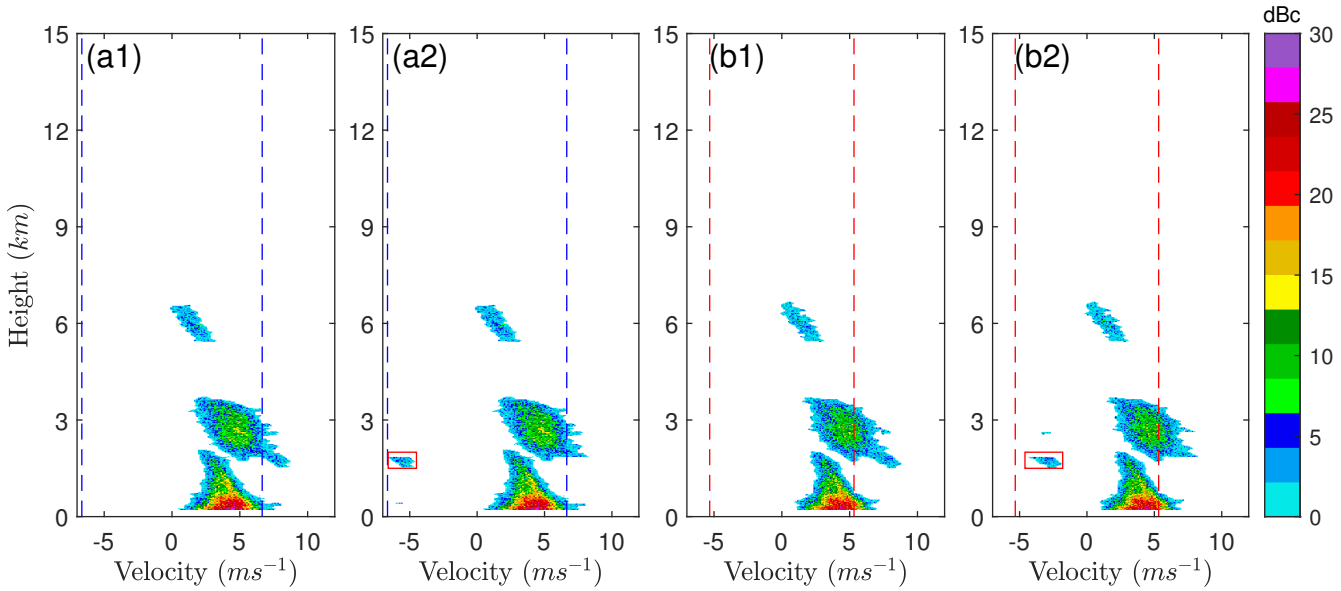


Figure 9. Comparison between the dealiased Doppler power spectrum by our method and Zheng's. (**a1**,**a2**) are the dealiased Doppler power spectrums for the high PRF by our method and Zheng's, respectively. (**b1**,**b2**) are the same but for the low PRF.

At the neighboring range gates, where the half-folding peak transformed into a full-folding peak, for convenience, we denote the unfolded peak as peak 1, and the peak that changes from half-folding to full-folding as peak 2. In the range gate with a half-folding peak 2, although the majority of peak 2 is in the negative interval, its negative part is folded back to the positive interval due to the successful determination of the half-folding. In the range gate with the full-folding peak 2, on the other hand, peak 2 is considered to be in the same Nyquist interval as peak 1. Assuming that there is almost no change in the shape and intensity of peak 1 and peak 2 between the two range gates, the calculated Doppler mean velocity is $w_1\overline{V}_1 + w_2(\overline{V}_2 + 2V_{max})$ and $w_1\overline{V}_1 + w_2\overline{V}_2$ for the half-folding and the full-folding range gates, respectively. $\overline{V}_1$ and $\overline{V}_2$ are the Doppler mean velocities of peak 1 and peak 2, respectively, in the primary Nyquist interval. w_1 and w_2 are the weight factors of peak 1 and peak 2 based on their total power, respectively. As a result, a sudden change of about $2V_{max}w_2$ occurred in Zheng's profile.

A slice at range gate 1.66 km in case B is used to illustrate the implementation of our spectral dealiasing method. Figure 10 shows the Doppler power spectrums before and after our spectral dealiasing. Initially, we found the presence of two peaks and there was no half-folding peak. Then, we determined the major peak and subpeak based on their power (amplitude). In the high PRF, the Doppler mean velocity of each peak was 3.13 and -5.37 m s^{-1} for the major peak and subpeak, respectively. In the low PRF, they were 3.17 and -2.76 m s^{-1}. The left distance from the major peak to the subpeak was 8.5 m s^{-1} in the high PRF, while the right distance was 4.79 m s^{-1}, which needed to cross the Nyquist interval according to $V^h_{max} = 6.65$. For the low PRF, the left and right distances were 5.94 and 4.70 m s^{-1}, respectively. The difference in the left distance between high and low PRFs was 2.56 m s^{-1}, where $2(V^h_{max} - V^l_{max})$ was 2.66 m s^{-1}. The difference in the right distance was 0.09 m s^{-1}. It was evident that the right distance was the true distance while the left distance was caused by Nyquist folding. It means that the subpeak had a higher velocity than the major peak and was located in a higher Nyquist interval. There was an implicit half-folding. Then, we selected split points in the interval of both left distances and moved the left segments to the right of V_{max}. Based on the new spectrum, we calculated the dealiased Doppler mean velocity. They were 4.08 and 4.53 m s^{-1} for high and low PRFs, respectively. In contrast, the original Doppler mean velocities were 1.44 and 1.46 m s^{-1}

for high and low PRFs, respectively. The difference between the original Doppler mean velocities was even smaller than the dealiased one.

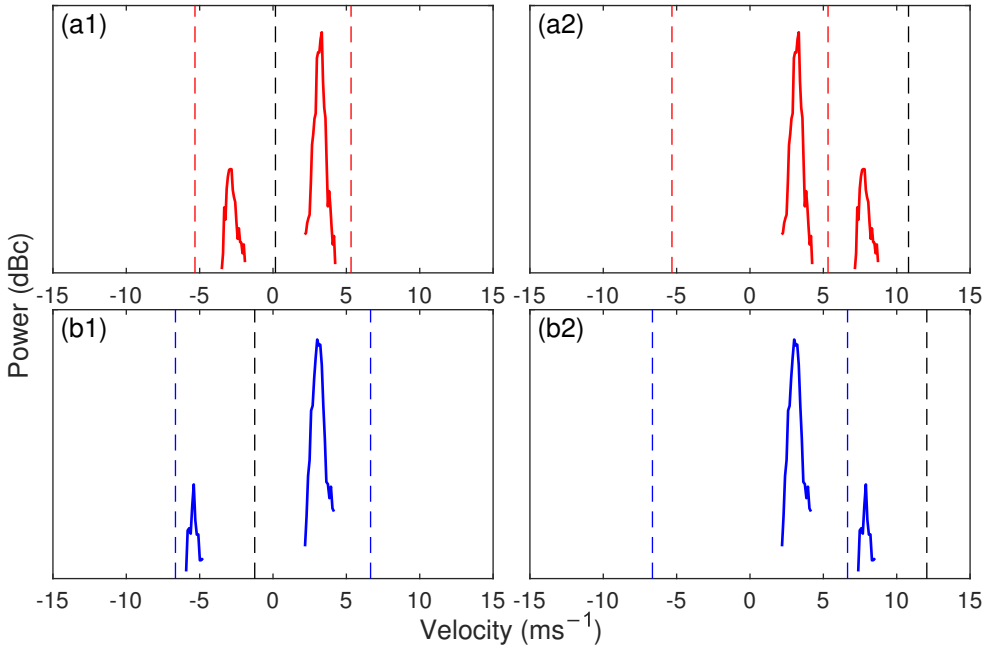


Figure 10. Example of Doppler spectrum before and after our spectral dealiasing processing. (**a1**,**a2**) denote the Doppler spectrum of the low PRF before and after dealiasing, respectively, while (**b1**,**b2**) denote the same for the high PRF.

6. Results and Discussion

In this section, some characteristics of half-folding in terms of individual Doppler mean velocity, Doppler spectral width, and the final velocity after dual-PRF processing are discussed. To validate our method, we also provide statistics based on the TJ-II observation.

Figure 11 shows the Doppler mean velocities for high and low PRFs by Zheng's spectral dealiasing method and ours. Compared to the unprocessed Doppler mean velocities shown in Figure 4, a large number of low-velocity results (near 0 m s^{-1}, in yellow) occurred in the region below 5 km in Figure 4 caused by half-folding where the positive and negative parts of the Doppler power spectrum cancel out. They were replaced by high-velocity results (either a high positive velocity in red or a high negative velocity in green) in our result, which is the indication of the half-folding being dealiased. Zheng's results still had some small regions around the time 17:00 and height of 1 km with bins in yellow, which is due to the inability to detect implicit half-folding. These regions with implicit half-folding, which Zheng's method cannot resolve, are more clearly visible in Figure 11(c1,c2).

Figure 12 shows the Doppler spectral widths for high and low PRFs by three spectral dealiasing methods. With the presence of half-folding, the Doppler spectral widths without spectral dealiasing were typically very large, such as the large red and purple regions in Figure 12a. There were also some small red regions in Figure 12c, indicating the occurrence of implicit half-folding that Zheng's method failed to address. Doppler spectral width maps allow one to intuitively determine where half-folding occurs, but when applied to algorithms, relying on Doppler spectral widths is not absolutely valid, either in absolute terms or in terms of the difference. In terms of absolute value, it is difficult to distinguish high-spectral-width results from half-folding when the true spectral width is also large. In terms of the difference, the difference of Doppler spectral width between high and low PRFs before spectral dealiasing is not always larger than the one after spectral dealiasing. In this TJ-II observation, there were 39946 bins where the Doppler spectral width difference between high and low PRFs before spectral dealiasing was larger than the difference after dealiasing, but there were still 1838 bins where it was smaller. In contrast, our

spectral dealiasing method is based on the physical property associated with dual PRFs, the consistency of the true velocity difference between peaks, which will not change with different folding cases, either explicit or implicit half-folding.

Figure 13 shows the final results of dual PRF processing with three different spectral dealiasing methods. In Figure 13a, there were a large number of color mutations representing the mutation of the Nyquist interval estimated by the dual PRF processing, such as the region around the time 16:53 and height of 1.5 km and the region around the time 17:00 and height of 1.5 km. Meanwhile, even in the regions with smooth color transitions where the estimated Nyquist intervals were correct and consistent, the deviation in the measured Doppler mean velocities caused by half-folding still led to incorrect results with large deviations, such as the region around the time 16:53 and height of 4.5 km compared to the same region in Figure 13b,c. For the results of Zheng's method as shown in Figure 13c, most dealiased velocities were the same as that of ours in Figure 13b. There remained small regions with velocity mutations, such as the region around the time 17:00 and height of 1 km. This was due to the presence of implicit half-folding in these regions, which cannot be detected and dealiased by Zheng's method. Since our method considers all cases of folding and can resolve them, there were no color mutations in our dealiased results in Figure 13b.

We may be able to summarize some characteristics of the half-folding from comparisons of the three results. However, even though we could detect the half-folding through these characteristics, we cannot fix the folded data. We cannot tell from the folded results how much the Doppler power spectrum has been folded. Therefore, half-folding must be detected and solved at the Doppler power spectrum.

Table 1 shows the statistics of aliasing cases in this observation. There were a total of 75,226 valid data bins from the TJ-II observation used in this section. For the high PRF, the aliasing occurred in about 35% of bins, 97.8% being half-folding and only 2.2% being full-folding. For the low PRF, the aliasing occurred in about 54% of bins, with 95.8% being half-folding and 4.2% being full-folding. Half-folding accounted for the vast majority of the total aliasing cases at both PRFs, while full-folding accounted for only a small percentage. This highlights the importance of paying attention to half-folding in vertically pointing MMCR. In half-folding cases, implicit half-folding had a non-negligible share of about 9% and 10% for high and low PRFs, respectively. Therefore, it is essential to consider implicit half-folding in spectral dealiasing.

Table 1. The number of bins with different folding cases for high and low PRFs.

PRF	Nonfolding	Half-Folding		Full-Folding
		Explicit	Implicit	
High	48,295	26,338		593
		23,951	2387	
Low	32,857	40,605		1764
		36,429	4176	

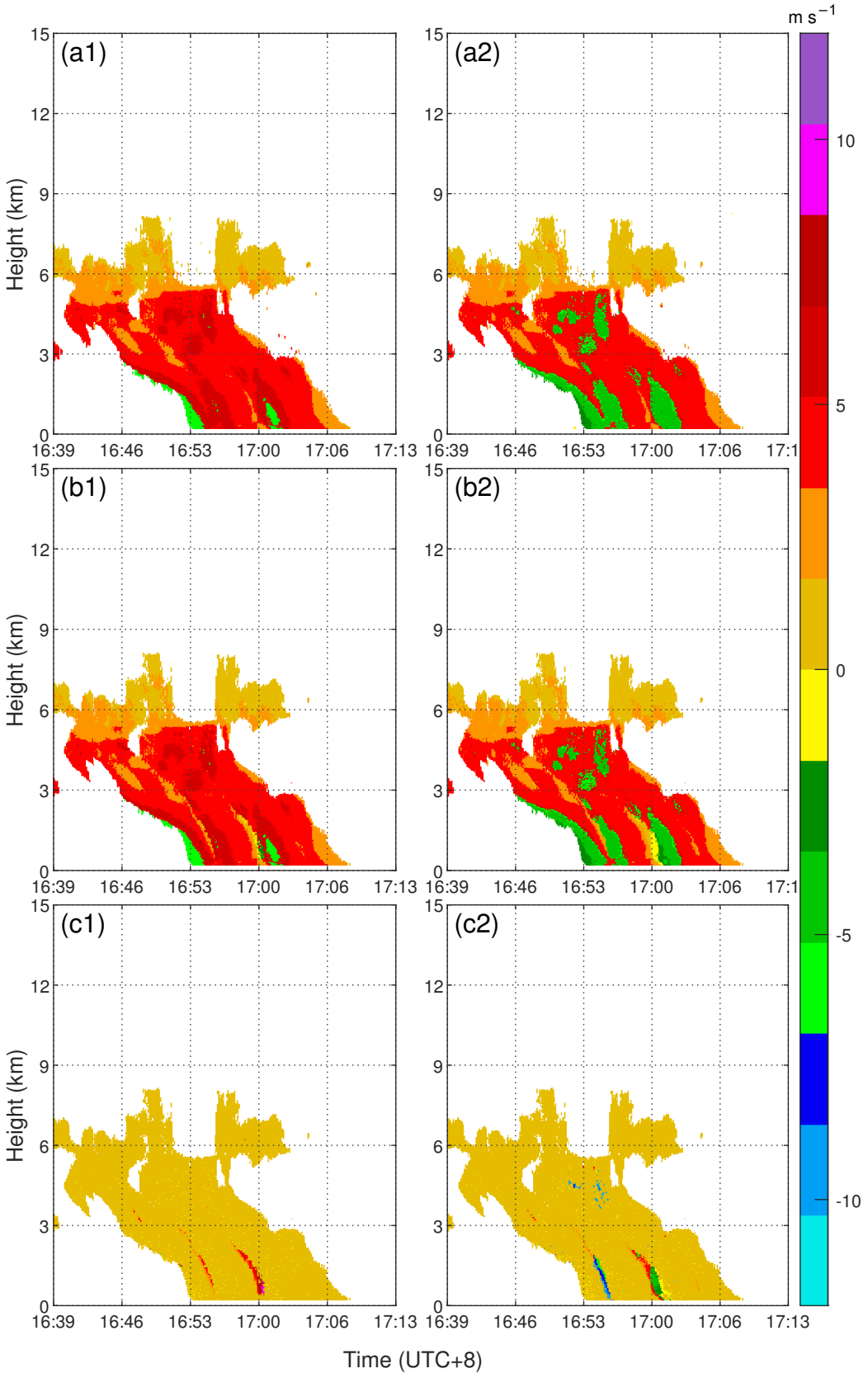


Figure 11. Doppler mean velocities for high and low PRFs by Zheng's spectral dealiasing method and ours. (**a1**,**a2**) are the results of our method for high and low PRFs, respectively. (**b1**,**b2**) are the results of Zheng's method. (**c1**,**c2**) are the differences between our method and Zheng's method for high and low PRFs, respectively.

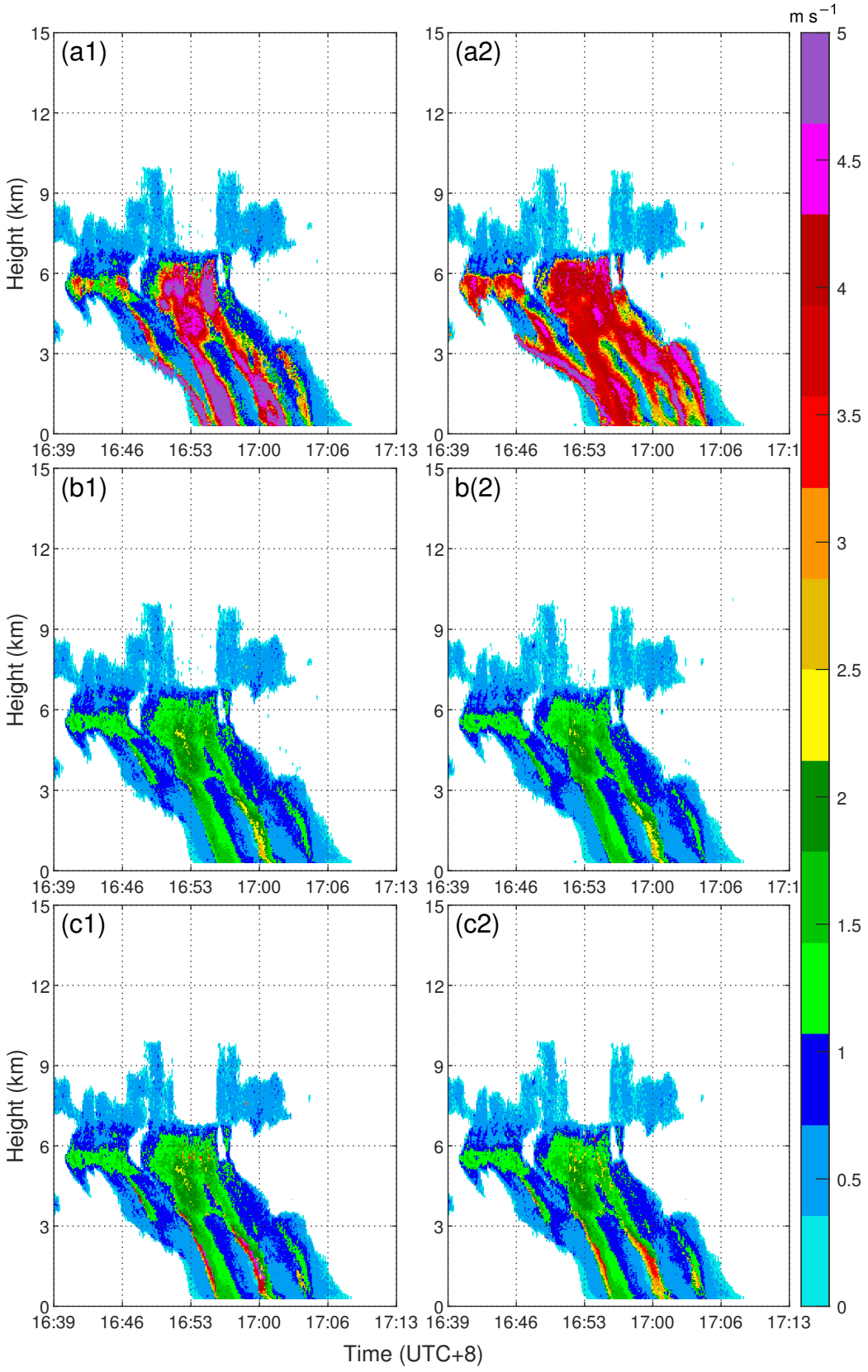


Figure 12. Doppler spectral widths for high and low PRFs by different spectral dealiasing methods. (**a1**,**a2**) are results without spectral dealiasing for high and low PRFs, respectively. (**b1**,**b2**) are the results of our method. (**c1**,**c2**) are the results of Zheng's method.

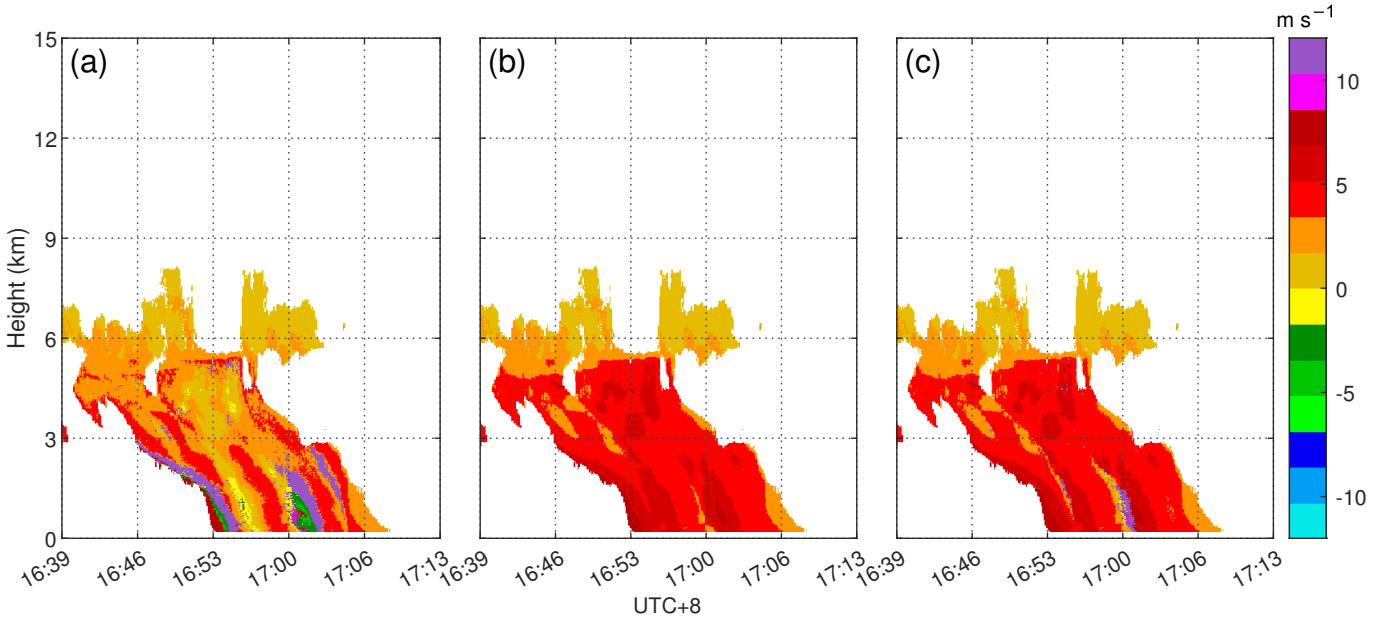


Figure 13. Dealiased velocity by dual PRFs with three different spectral dealiasing methods: (**a**) unprocessed, (**b**) our method (**c**), Zheng's method.

Table 2 shows the number of bins with correct velocities obtained by dual-PRF postprocessing after different spectral dealiasing. Dual-PRF processing without spectral deliasing only solved 33,448 bins, even less than the nonfolding bins in the high PRF. This is because the results of the dual-PRF processing are jointly determined by both high and low PRFs. If a half-folding occurs in the Doppler power spectrum of either PRF, the final result of the dual-PRF processing will be incorrect. For example, it is common for the Doppler power spectrum of the low PRF to be half-folding when the spectrum of the high PRF is still nonfolding, causing the measured Doppler mean velocity of the low PRF to deviate significantly from the true velocity, which in turn incorrectly predicts the Nyquist interval during dual-PRF processing. The same issue also occurs when the Doppler power spectrum of the low PRF is already full-folding while the spectrum of the high PRF is still half-folding. Without spectral dealiasing, dual-PRF processing only works when the Doppler power spectrums of both high and low PRFs are full-folding compared to the single PRF. However, full-folding only takes a small amount compared to half-folding according to the statistics. In other words, applying the dual-PRF processing without spectral dealiasing may instead cause a decrease in usability.

Table 2. The number of bins with correct dealiased velocities by different spectral dealiasing methods.

Unprocessed	Zheng's Method	Our Method
33,448	70,537	75,226

The usability of the dual-PRF processing in vertically pointing MMCR improved at once with the presence of spectral dealiasing, as shown in Table 2 with Zheng's method and ours. There were still some incorrect results in Zheng's method. When implicit half-folding occurred, Zheng's method did not detect the presence of implicit half-folding, which in turn led to failure. Our method, on the other hand, effectively detected and solved the implicit half-folding by introducing the property of the dual PRFs into the spectral dealiasing. Therefore, we had 4689 more correct bins than Zheng's method where the implicit folding occurred in either high or low PRFs. In terms of the 41,778 bins that needed spectral dealiasing, our method was able to improve the success rate by 11.2% over Zheng's method.

7. Conclusions

Half-folding, a special case of velocity aliasing in vertically pointing MMCR, invalidates many conventional postprocessing methods for weather radars by breaking the principle of dealiasing in Equation (2). Half-folding must be resolved before the Doppler mean velocity can be calculated. There are several spectral dealiasing methods capable of resolving the half-folding, but some of them do not fully consider the special cases, i.e., the implicit half-folding in the case of two peaks. Some of them do consider the two-peak cases, but they are mostly based on some empirical assumptions that fail under certain conditions and are therefore not reliable enough. We proposed a reliable velocity dealiasing method for vertically pointing MMCR based on the dual-PRF technique, and of course, taking into account half-folding. Our method consisted of two stages. One was the spectral dealiasing before calculating the Doppler moments, and the other was the conventional dual-PRF processing after calculating the Doppler moments. Both stages took full advantage of the dual-PRF technique. In the spectral dealiasing, we used the consistency of the velocity difference between peaks in different PRFs to resolve the half-folding with two peaks, including implicit half-folding. After obtaining the proper Doppler mean velocity that obeyed the dealiasing principle, we performed the regular dual-PRF processing. The high reliability of our method was demonstrated by TJ-II observations.

Author Contributions: H.L. designed the algorithm and wrote the paper under the guidance of J.G.; H.L. and J.W. were in charge of radar observation experiments; J.G. was in charge of the whole project. All authors have read and agreed to the published version of the manuscript. All authors have read and agreed to the published version of the manuscript.

Funding: This research was funded by the National Natural Science Foundation of China (grant No. 61671249) and the Jiangsu Innovation and Entrepreneurship Group Talents Plan.

Data Availability Statement: Data related to this article are available upon request to the corresponding author.

Conflicts of Interest: The authors declare no conflict of interest.

References

1. Stephens, G.L.; Tsay, S.C.; Stackhouse, P.W.; Flatau, P.J. The Relevance of the Microphysical and Radiative Properties of Cirrus Clouds to Climate and Climatic Feedback. *J. Atmos. Sci.* **1990**, *47*, 1742–1754. [CrossRef]
2. Arking, A. The Radiative Effects of Clouds and their Impact on Climate. *Bull. Am. Meteorol. Soc.* **1991**, *72*, 795–813. [CrossRef]
3. Battan, L.J. Some Observations of Vertical Velocities and Precipitation Sizes in a Thunderstorm. *J. Appl. Meteorol.* **1964**, *3*, 415–420. [CrossRef]
4. McLinden, M.L.W.; Li, L.; Heymsfield, G.M.; Coon, M.; Emory, A. The NASA GSFC 94-GHz Airborne Solid-State Cloud Radar System (CRS). *J. Atmos. Ocean. Technol.* **2021**, *38*, 1001–1017. [CrossRef]
5. Lhermitte, R. A 94-GHz Doppler Radar for Cloud Observations. *J. Atmos. Ocean. Technol.* **1987**, *4*, 36–48. [CrossRef]
6. Marchand, R.; Mace, G.G.; Ackerman, T.; Stephens, G. Hydrometeor Detection Using Cloudsat—An Earth-Orbiting 94-GHz Cloud Radar. *J. Atmos. Ocean. Technol.* **2008**, *25*, 519–533. [CrossRef]
7. Clothiaux, E.E.; Miller, M.A.; Albrecht, B.A.; Ackerman, T.P.; Verlinde, J.; Babb, D.M.; Peters, R.M.; Syrett, W.J. An Evaluation of a 94-GHz Radar for Remote Sensing of Cloud Properties. *J. Atmos. Ocean. Technol.* **1995**, *12*, 201–229. [CrossRef]
8. Kollias, P.; Clothiaux, E.E.; Miller, M.A.; Albrecht, B.A.; Stephens, G.L.; Ackerman, T.P. Millimeter-Wavelength Radars: New Frontier in Atmospheric Cloud and Precipitation Research. *Bull. Am. Meteorol. Soc.* **2007**, *88*, 1608–1624. [CrossRef]
9. Görsdorf, U.; Lehmann, V.; Bauer-Pfundstein, M.; Peters, G.; Vavriv, D.; Vinogradov, V.; Volkov, V. A 35-GHz Polarimetric Doppler Radar for Long-Term Observations of Cloud Parameters—Description of System and Data Processing. *J. Atmos. Ocean. Technol.* **2015**, *32*, 675–690. [CrossRef]
10. Andronache, C. *Remote Sensing of Clouds and Precipitation*; Springer International Publishing: Berlin/Heidelberg, Germany, 2018. [CrossRef]
11. Ray, P.S.; Ziegler, C. De-Aliasing First-Moment Doppler Estimates. *J. Appl. Meteorol.* **1977**, *16*, 563–564. [CrossRef]
12. Bergen, W.R.; Albers, S.C. Two- and Three-Dimensional De-aliasing of Doppler Radar Velocities. *J. Atmos. Ocean. Technol.* **1988**, *5*, 305–319. [CrossRef]
13. Eilts, M.D.; Smith, S.D. Efficient Dealiasing of Doppler Velocities Using Local Environment Constraints. *J. Atmos. Ocean. Technol.* **1990**, *7*, 118–128. [CrossRef]
14. Jing, Z.; Wiener, G. Two-Dimensional Dealiasing of Doppler Velocities. *J. Atmos. Ocean. Technol.* **1993**, *10*, 798–808. [CrossRef]

15. James, C.N.; Houze, R.A. A Real-Time Four-Dimensional Doppler Dealiasing Scheme. *J. Atmos. Ocean. Technol.* **2001**, *18*, 1674–1683. [CrossRef]
16. Haase, G.; Landelius, T. Dealiasing of Doppler Radar Velocities Using a Torus Mapping. *J. Atmos. Ocean. Technol.* **2004**, *21*, 1566–1573. [CrossRef]
17. Xu, Q.; Nai, K.; Wei, L.; Zhang, P.; Liu, S.; Parrish, D. A VAD-Based Dealiasing Method for Radar Velocity Data Quality Control. *J. Atmos. Ocean. Technol.* **2011**, *28*, 50–62. [CrossRef]
18. Ferrari, A.; Berenguer, C.; Alengrin, G. Doppler ambiguity resolution using multiple PRF. *IEEE Trans. Aerosp. Electron. Syst.* **1997**, *33*, 738–751. [CrossRef]
19. Crum, T.D.; Alberty, R.L. The WSR-88D and the WSR-88D Operational Support Facility. *Bull. Am. Meteorol. Soc.* **1993**, *74*, 1669–1687. [CrossRef]
20. Doviak, R.J.; Bringi, V.; Ryzhkov, A.; Zahrai, A.; Zrnić, D. Considerations for Polarimetric Upgrades to Operational WSR-88D Radars. *J. Atmos. Ocean. Technol.* **2000**, *17*, 257–278. [CrossRef]
21. Jorgensen, D.P.; Shepherd, T.R.; Goldstein, A.S. A Dual-Pulse Repetition Frequency Scheme for Mitigating Velocity Ambiguities of the NOAA P-3 Airborne Doppler Radar. *J. Atmos. Ocean. Technol.* **2000**, *17*, 585–594. [CrossRef]
22. Maahn, M.; Kollias, P. Improved Micro Rain Radar snow measurements using Doppler spectra post-processing. *Atmos. Meas. Tech.* **2012**, *5*, 2661–2673. [CrossRef]
23. Zheng, J.; Liu, L.; Zeng, Z.; Xie, X.; Wu, J.; Feng, K. Ka-band millimeter wave cloud radar data quality control. *J. Infrared Millim. Waves* **2016**, *35*, 748. [CrossRef]
24. Garcia-Benadi, A.; Bech, J.; Gonzalez, S.; Udina, M.; Codina, B.; Georgis, J.F. Precipitation Type Classification of Micro Rain Radar Data Using an Improved Doppler Spectral Processing Methodology. *Remote Sens.* **2020**, *12*, 4113. [CrossRef]
25. Lin, H.; Wang, J.; Chen, Z.; Ge, J. A 94 GHz Pulse Doppler Solid-State Millimeter-Wave Cloud Radar. *Remote Sens.* **2023**, *15*, 3098. [CrossRef]
26. Dazhang, T.; Geotis, S.G.; Passarelli, R.E.; Hansen, A.L.; Frush, C.L. Evaluation of an alternating-prf method for extending the range of unambiguous doppler velocity. In Proceedings of the 22nd Conference on Radar Meteorology, Zurich, Switzerland, 10–13 September 1984.
27. Holleman, I.; Beekhuis, H. Analysis and Correction of Dual PRF Velocity Data. *J. Atmos. Ocean. Technol.* **2003**, *20*, 443–453. [CrossRef]
28. Shupe, M.D.; Kollias, P.; Matrosov, S.Y.; Schneider, T.L. Deriving Mixed-Phase Cloud Properties from Doppler Radar Spectra. *J. Atmos. Ocean. Technol.* **2004**, *21*, 660–670. [CrossRef]
29. Kalesse, H.; Vogl, T.; Paduraru, C.; Luke, E. Development and validation of a supervised machine learning radar Doppler spectra peak-finding algorithm. *Atmos. Meas. Tech.* **2019**, *12*, 4591–4617. [CrossRef]
30. Schimmel, W.; Kalesse-Los, H.; Maahn, M.; Vogl, T.; Foth, A.; Garfias, P.S.; Seifert, P. Identifying cloud droplets beyond lidar attenuation from vertically pointing cloud radar observations using artificial neural networks. *Atmos. Meas. Tech.* **2022**, *15*, 5343–5366. [CrossRef]
31. Kalesse-Los, H.; Schimmel, W.; Luke, E.; Seifert, P. Evaluating cloud liquid detection against Cloudnet using cloud radar Doppler spectra in a pre-trained artificial neural network. *Atmos. Meas. Tech.* **2022**, *15*, 279–295. [CrossRef]

Disclaimer/Publisher's Note: The statements, opinions and data contained in all publications are solely those of the individual author(s) and contributor(s) and not of MDPI and/or the editor(s). MDPI and/or the editor(s) disclaim responsibility for any injury to people or property resulting from any ideas, methods, instructions or products referred to in the content.